Supporting Information

Exploring the segregating and mineralization-inducing capacities of cationic hydrophilic polymers for preparation of robust, multi-functional mesoporous hybrid microcapsules

Jiafu Shi, Wenyan Zhang, Xiaoli Wang, Zhongyi Jiang, Shaohua Zhang, Xiaoman Zhang, Chunhong Zhang, Xiaokai Song, Qinghong Ai*

Key Laboratory for Green Chemical Technology of Ministry of Education, School of Chemical Engineering and Technology, Tianjin University, Tianjin 300072, China.

E-mail: zhyjiang@tju.edu.cn; Fax: 86-22-23500086; Tel: 86-22-23500086

1. Results and discussion

Table S1. Synthesizing conditions and mechanical strength of PGTi microcapsules[a].

Capsule name	GA concentration /*wt*%	Crosslinking time /min	Ti-BALDH concentration /mM	Template synthesizing temperature /°C	Mechanical strength[b]	
					Broken ratio/%	Deformed ratio/%
PGTi-1	0.01	60	50	20	0	0
PGTi-2	0.05	60	50	20	0	0.8
PGTi-3	0.1	60	50	20	0	6.4
PGTi-4	0.2	60	50	20	0	20
PGTi-5	0.5	60	50	20	0	42.4
PGTi-6	1.0	60	50	20	0	64.8
PGTi-7	2.0	60	50	20	0	79.6
PGTi-8	0.01	10	50	20	0	17.2
PGTi-9	0.01	30	50	20	0	8.8
PGTi-10	0.01	120	50	20	0	28.4
PGTi-11	0.01	240	50	20	0	——
PGTi-12	0.01	60	5	20	0	94.8
PGTi-13	0.01	60	10	20	0	50.4
PGTi-14	0.01	60	100	20	0	0
PGTi-15	0.01	60	50	10	0	0
PGTi-16	0.01	60	50	40	0	0

[a] Synthesis condition: PAH, M_w: 70 kDa, concentration: 2 mg mL^{-1}.

[b] The mechanical strength of PGTi microcapsules is investigated by the method of osmotic induced invagination (PGTi microcapsules are dispersed in 20 (*w/v*)% PSS aqueous solutions with vigorously stirring for 6 h).[R1]

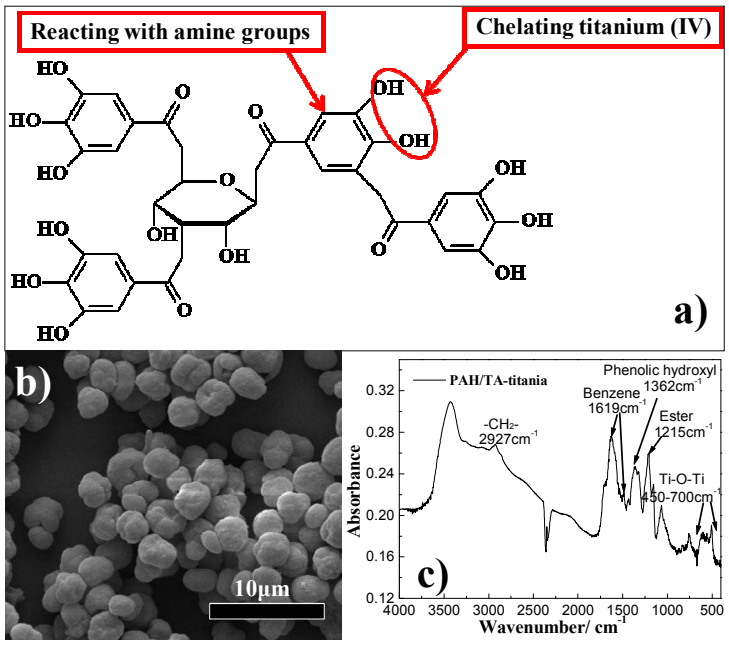

Figure S1. a) Chemical structure of tannic acid (TA); b) SEM image and c) FTIR spectrum of PAH/TA-titania microcapsules. (PAH, M_w: 70 kDa, concentration: 2 mg mL^{-1})

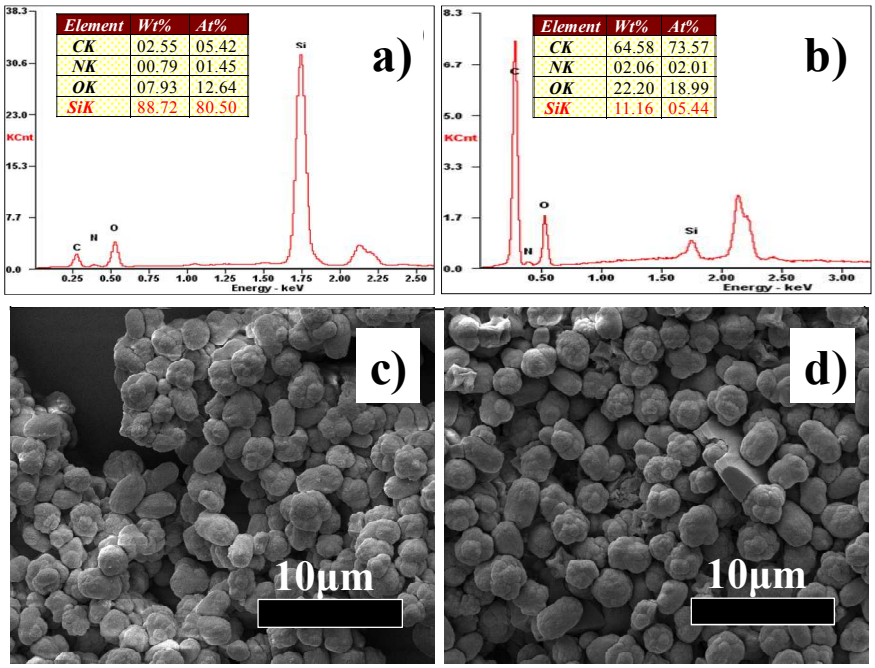

Figure S2. EDS spectra and SEM images of a,e) PAH/GA-silica and b,f) PAH/TA-silica microcapsules. (PAH, M_w: 70 kDa, concentration: 2 mg mL^{-1})

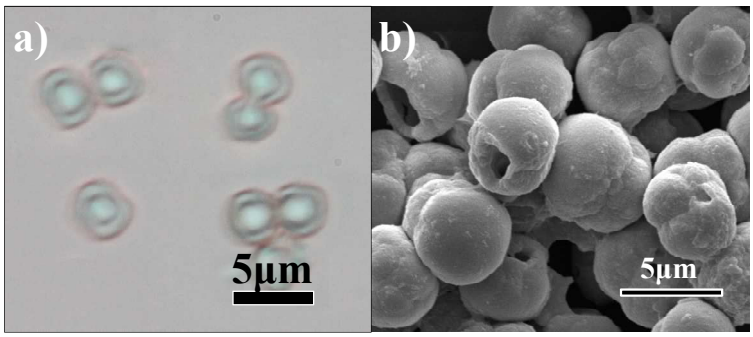

Figure S3. a) Optical image and b) SEM image of PGTi-1 microcapsules. (PAH, Mw: 70 kDa, concentration: 2 mg mL^{-1})

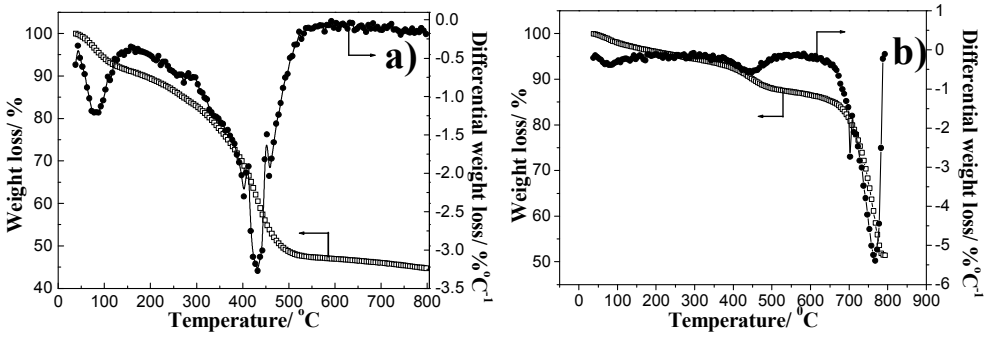

Figure S4. TG and DTG analysis of a) PGTi-$CaCO_3$ microspheres and b) PGTi microcapsules. (PAH, M_w: 70 kDa, concentration: 2 mg mL^{-1})

Thermo-gravimetric (TG) and derivative thermo-gravimetric (DTG) analysis are conducted to assess the temperature-weight loss profile and the percentage of inorganic component in PGTi microcapsules. As shown in Figure S4a, PGTi microcapsules exhibit an endothermic peak at *ca.* 100 °C, attributing to water evaporation.[R2] And the endothermic peaks at *ca.* 425 °C should be ascribed to the decomposition of organics[R3] (PAH and GA). Compared to the DTG curve of PGTi-$CaCO_3$ microspheres (Figure S4b), the peak of PGTi microcapsules at 750 °C disappears, indicating the complete removal of $CaCO_3$. The final inorganic content in PGTi microcapsules is 44.8 *wt*%.

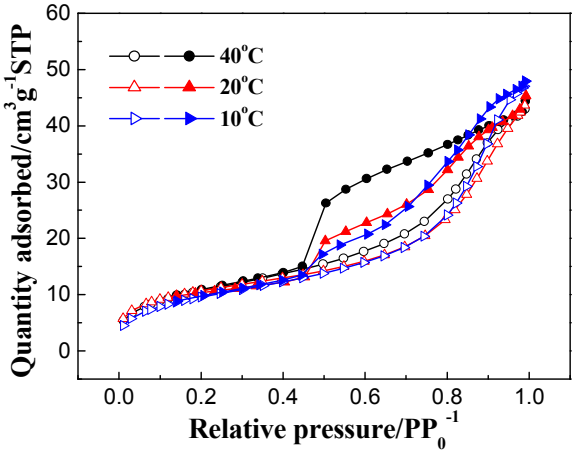

Figure S5. N_2 adsorption-desorption isotherm of P-$CaCO_3$ microspheres as a function of synthesizing temperature. (PAH, M_w: 70 kDa, concentration: 2 mg mL^{-1})

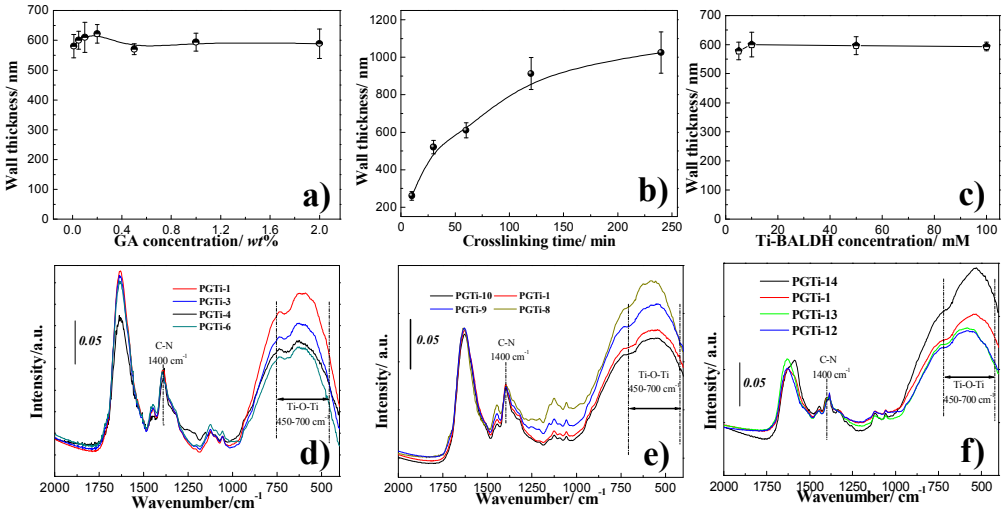

Figure S6. a-c) Wall thickness and d-f) FTIR spectra of PGTi microcapsules as a function of a,d) crosslinking time, b,e) GA concentration, and c,f) Ti-BALDH concentration. (PAH, M_w: 70 kDa, concentration: 2 mg mL^{-1})

Precise control of wall thickness, morphology as well as mechanical strength of the capsule is also essential for synthesis of PGTi microcapsules. (*Herein, the wall thickness was measured by high-resolution scanning electron microscopy (HRSEM). The maximum magnification of HRSEM is 8000.*) Therefore, the effect of GA concentration, crosslinking time and Ti-BALDH concentration are explored. In Figure S6a-S6c, the capsule wall thickness is influenced slightly by either GA concentration or Ti-BALDH concentration, keeping a nearly constant wall thickness of *ca.* 600 nm. However, when prolonging the crosslinking time from 10 to 240 min, the wall thickness increases from *ca.* 250 to 1000 nm. Generally, longer crosslinking time could lead to deeper penetration of GA into P-$CaCO_3$ microspheres, resulting in thicker GA-crosslinked PAH layer and thus thicker hybrid capsule wall. As the crosslinking time is prolonged from 120 to 240 min, the capsule wall preserves a constant thickness as a result of the inherent near-surface enrichment of PAH in P-$CaCO_3$ microspheres.[R4, R5] Theoretically, the maximum wall thickness of PGTi microcapsules should be the thickness of crosslinked PAH layer within P-$CaCO_3$ microspheres. Therefore, too longer crosslinking time would not increase the capsule wall thickness. Meanwhile, increasing GA concentration facilitates to form "erythrocyte-like" microcapsules with an umbilicate morphology (Figure S7). Accordingly, the deformed ratio of microcapsules increases from 79.6 to 0% with the increase of GA concentration from 0.01 to 2.0 *wt*% (Table 1 in the manuscript). From the reaction mechanism between amine and aldehyde groups, increasing GA concentration consumes more amino groups, which imparts a reduced amount of titania

(Figure S6e), leading to a decreased mechanical strength of the microcapsules. However, an interesting phenomenon happens as the crosslinking time alters: although the titania amount increases as crosslinking time is prolonged, the maximum amount of titania does not endow the most robust morphology, and the least deformed ratio of microcapsules was obtained at 60 min crosslinking time (Figure S8 and Table 1 in the manuscript). This is because that the short-time crosslinking of PAH and GA only takes place adjacent to surface. Most of PAH is still in free state, which may endow a more flexible structure even though more amount of titania has been generated. Changing the Ti-BALDH concentration would also affect the microcapsule morphology and mechanical strength. Figure S9 shows that the aggregation degrees of microcapsules decrease gradually with the increase of Ti-BALDH concentration. Meanwhile, at lower Ti-BALDH concentration (5 and 10 mM), most of microcapsules collapse or deform, while at higher Ti-BALDH concentration (50 and 100 mM), the mechanical strength of microcapsules is dramatically enhanced, resulting in intact spherical morphology. This phenomenon could be explained as that Ti-BALDH of higher concentrations could generate more amount of titnaia, leading to higher inorganic-to-organic ratio as evidenced in FTIR curves (Figure S6f). Note that although deformed microcapsules exist in some types of PGTi microcapsules, no broken microcapsules could be found (Table S1).

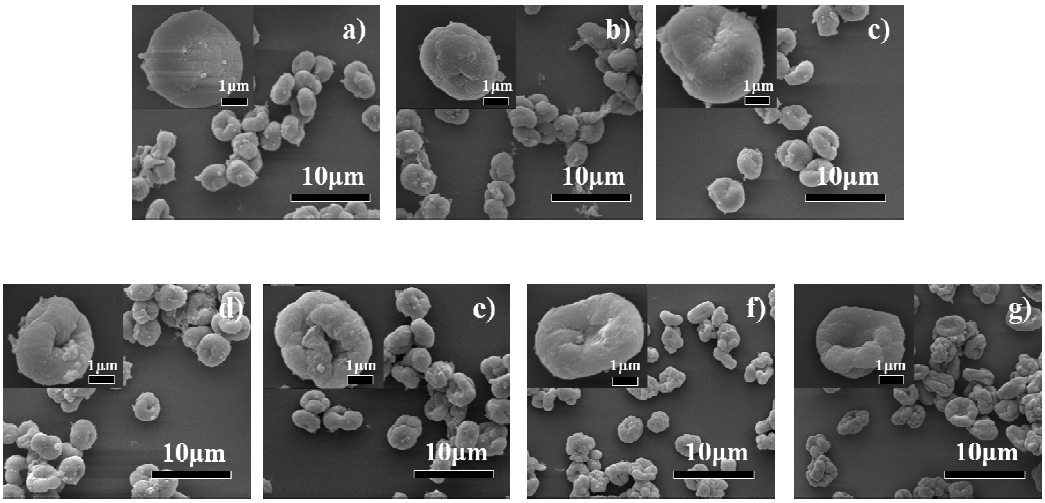

Figure S7. SEM images of PGTi microcapsules incubated in GA aqueous solution with a concentration of a) 0.01, b) 0.05, c) 0.10, d) 0.20, e) 0.50, f) 1.00, and g) 2.00 *wt*%. (PAH, M_w: 70 kDa, concentration: 2 mg mL^{-1})

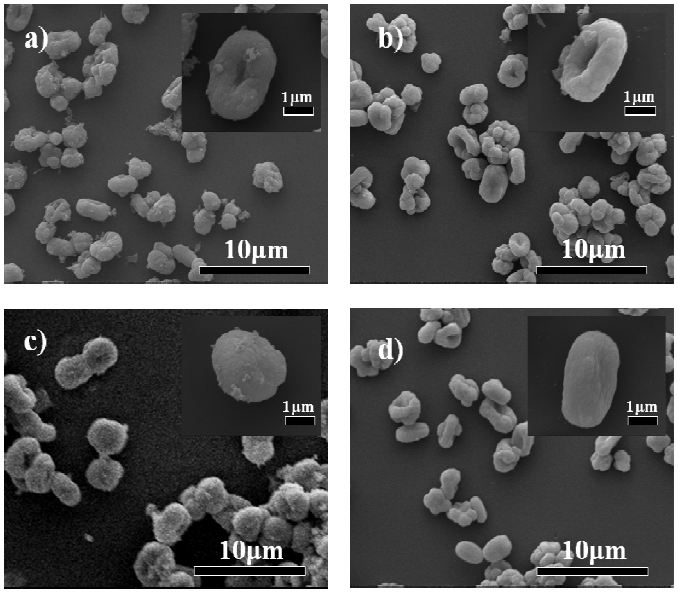

Figure S8. SEM images of PGTi microcapsules incubated in GA aqueous solution for a) 10, b) 30, c) 60, and d) 120 min. (PAH, M_w: 70 kDa, concentration: 2 mg mL^{-1})

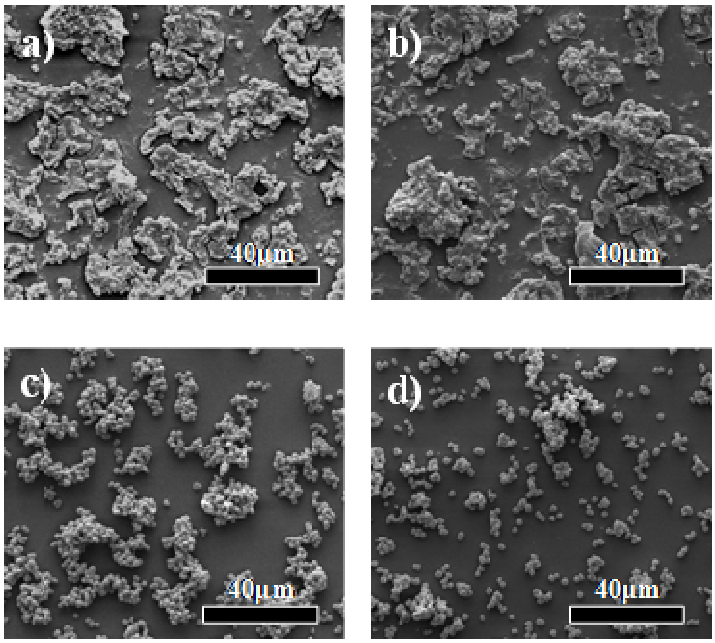

Figure S9. SEM images of PGTi microcapsules incubated in Ti-BALDH solution with a concentration of a) 5, b) 10, c) 50, and d) 100 mM. (PAH, M_w: 70 kDa, concentration: 2 mg mL^{-1})

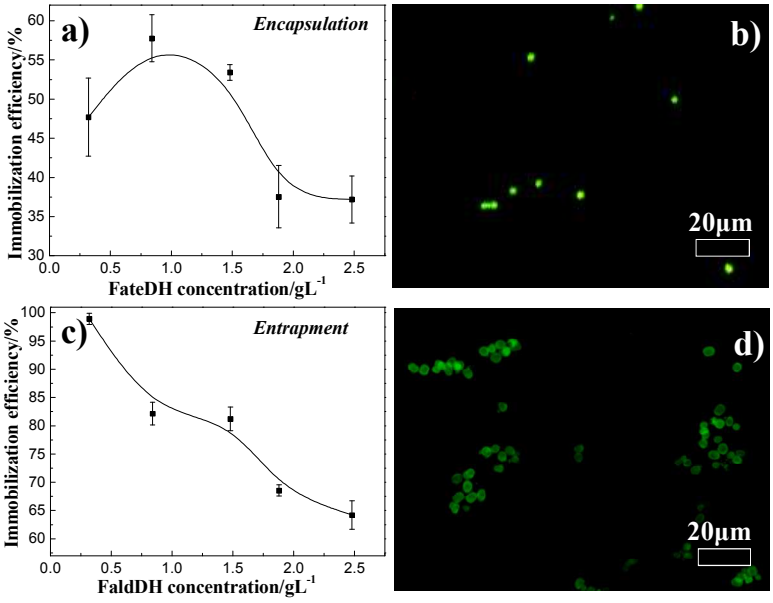

Figure S10. a) Encapsulation efficiency of FateDH and c) entrapment efficiency of FaldDH in PGTi microcapsules; florescence image of b) FateDH-encapsulated PGTi microcapsules and d) FaldDH-entapped PGTi microcapsules. (PAH, M_w: 70 kDa, concentration: 2 mg mL^{-1})

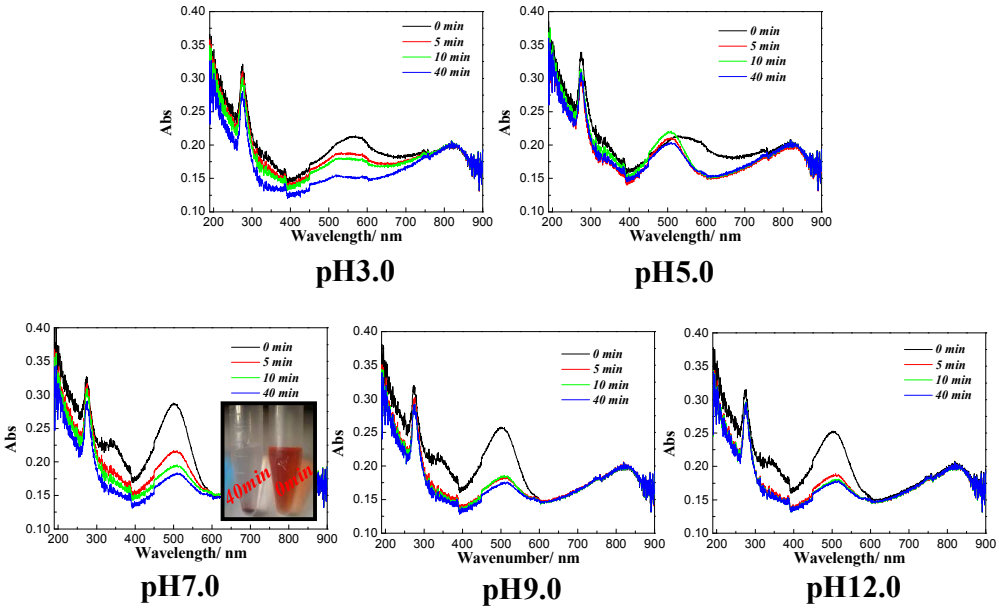

Figure S11. GR adsorption capability on PGTi-1 microcapsules as a function of pH value. (PAH, M_w: 70 kDa, concentration: 2 mg mL^{-1})

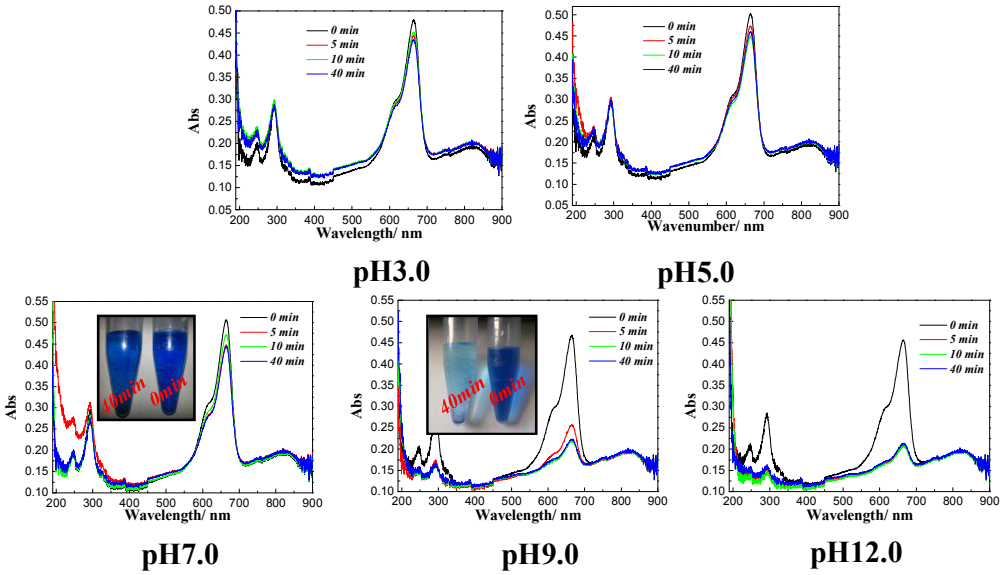

Figure S12. MB adsorption capability on PGTi-1 microcapsules as a function of pH value. (PAH, M_w: 70 kDa, concentration: 2 mg mL^{-1})

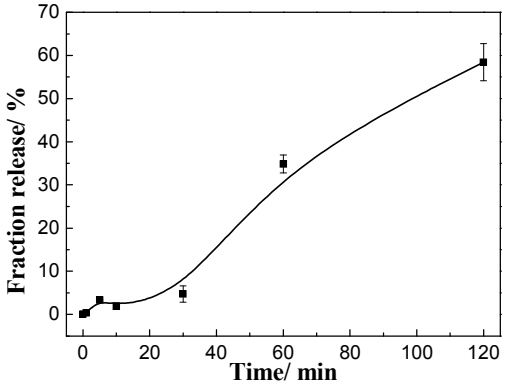

Figure S13. Release profile of MB for PGTi-1 microcapsules as a function of time (pH 7.0). (PAH, M_w: 70 kDa, concentration: 2 mg mL^{-1})

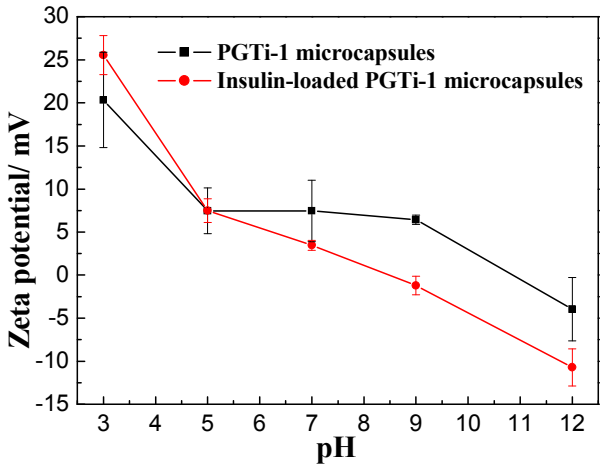

Figure S14. Surface zeta potential of PGTi-1 and insulin-loaded microcapsules as a function of pH value.

(PAH, M_w: 70 kDa, concentration: 2 mg mL^{-1})

R1. Feng, Z. Q.; Wang, Z. P.; Gao, C. Y.; Shen, J. C. *Adv. Mater.* **2007**, 19, 3687-3691.

R2. Jiang, Y. J.; Yang, D.; Zhang, L.; Li, L.; Sun, Q. Y.; Zhang, Y. F.; Li, J.; Jiang, Z. Y. *Dalton Trans*. **2008**, 4165-4171.

R3. Bagaria, H. G.; Kadali, S. B.; Wong, M. S. *Chem. Mater*. **2011**, *23*, 301-308.

R4. Wang, Z. P.; Mo□hwald, H.; Gao, C. Y. *Langmuir* **2011**, *27*, 1286-1291.

R5. Wang, Z. P.; Mohwald, H.; Gao, C. Y. *ACS Nano* **2011**, *5*, 3930-3936.